Study of Curved Beam Based Displacement Amplifying Compliant Mechanism for Accelerometer Design

Mithlesh Kumar[1(✉)] , P. Krishna Menon[2], and Ashok Kumar Pandey[1]

[1] Mechanical and Aerospace Engineering, Indian Institute of Technology Hyderabad, Kandi, Sangareddy, Telangana, India 502285
mithlesh.ece@gmail.com ,
ashok@mae.iith.ac.in
[2] Research Centre Imarat, Hyderabad 500069, India
https://people.iith.ac.in/ashok/

Abstract. The performance of an inertial micro-device largely depends on its displacement sensitivity. Different techniques like mechanical amplification using compliant mechanisms, geometric anti-spring design, and mode-localized can be employed for improving it. In this paper, a compliant mechanism-based accelerometer is studied and the design is optimized by incorporating a curved shaped beam. A detailed analysis presents interesting insight about the operation of the curved-shaped displacement amplifying compliant mechanism (DaCM). Study suggest that a larger sense mass displacement could also be achieved by DaCM with smaller geometrical amplification. The design simulations are carried out in finite element analysis (FEA) based CoventorWare and COMSOL Multiphysics simulator.

Keywords: Accelerometer · Displacement amplification · Compliant mechanism · Geometric anti-spring · MEMS

1 Introduction

Microelectromechanical systems (MEMS) have been of significant interest for design of inertial sensors because of their low cost, small size, and ruggedness. Devices like MEMS accelerometer and gyroscope find applications in consumer electronics, automobiles, missiles, aircraft navigation [1]. Applications like inertial navigation system for ships, aircraft, submarines, guided missiles, and spacecraft requires very high sensitivity and resolution (of an order of $10-20\,\mu g$

for accelerometer and $1-5°$/h for gyroscopes) [2]. Resolution of inertial MEMS devices is mainly limited by Brownian noise in micro-mechanical structures and interface electronics circuit noise [3]. A low mechanical sensitivity of MEMS devices may cause the electronics noise to dominate and limit the resolution [4]. Thus, there has been a significant interest to increase the sensitivity of MEMS. Different techniques like mechanical amplification using compliant mechanism, geometric anti-spring design, mode-localized design are being explored to improve the performance [5–7].

A compliant mechanism consists of flexible members that undergo deformation for applied force [8]. The deformation stores elastic energy in the flexible member, similar to strain energy in a deflected spring, which can be transferred or transformed to obtain a desired force-deflection relationship. In contrast, a rigid body mechanism consists of rigid link connected at movable joints to achieve a required force displacement behaviour. Thus, compared to a rigid body mechanism, a compliant structure has significantly lesser number of parts and movable joints to accomplish a specified task. Thus, it increases the precision of the compliant structures. Other advantages include miniaturization and reduction in weight of the compliant structure [8]. Further, compliant mechanism based design also suits the micro-fabrication process. It has allowed implementation of various compliant mechanism based MEMS devices like microgripper, crimping mechanism, compliant pliers [8]. The feasibility of micro-fabricated compliant structure has attracted research interest toward improving the displacement sensitivity of MEMS accelerometer; which can significantly improve their performance. In [9], a micro-lever based displacement amplifying mechanism was proposed for MEMS accelerometer. The lever mechanism works on the principle of displacement amplification at the free end of a beam for an applied force applied near to the fixed end of a beam as shown in Fig. 1(a). It shows a significant amplification of the output displacement and sensitivity. A simplest compliant structure for displacement amplification is an angled shaped beam shown in Fig. 1(b) [10]. The folded shape allow realization of amplification mechanism in smaller area. Different designs of displacement amplifying compliant mechanism have been studied in literature for accelerometer design [5,11,12].
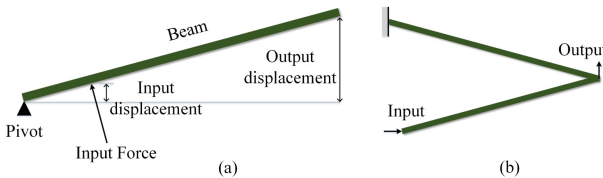

Fig. 1. Output displacement amplification: (a) lever mechanism [9], and (b) a simple compliant mechanism [10]

Applications like gravimeter for distributed gravity monitoring requires ultra-sensitive seismic accelerometer [6,13–15]. These accelerometers employ a curved shaped geometric anti-spring having reduced stiffness and very high sensitivity. In the present paper, the geometric anti-spring is incorporated in the design of displacement amplifying compliant mechanism and studied for its performance improvement. The designed accelerometer is also compared with the conventional accelerometer.

This article is organized as follows: A brief discussion on the design of conventional and compliant-mechanism accelerometer is presented in Sect. 2. Next, the optimization of displacement amplifying compliant mechanism is presented in Sect. 3. This is followed by the design and study of accelerometer with geometric anti-spring based compliant mechanism in Sect. 4. In the end, result and discussion is presented.

2 Accelerometer Designs

In this section, discussion on conventional (without mechanical amplification), and DaCM-based accelerometers are presented. In the following section, a novel design of DaCM is explored towards its performance improvement. The performance improvement by employing a DaCM in a design must not be at a cost of device footprint area. Thus, all designs considered in the manuscript have the same footprint area of $2\,\text{mm} \times 3\,\text{mm}$.

2.1 Conventional Accelerometer

A conventional accelerometer consist of a proof mass suspended for four springs at the corner such that the mass undergoes displacement in response to external vibrations. This allows displacement of combs attached to the proof mass and result in sense gap variations with respect to fixed combs attached to the substrate. A measure of this sense gap variations determine the acceleration of the external vibration. A conventional accelerometer is schematically illustrated in Fig. 2. The resonant frequency of the structure is 5.76 kHz and has a static displacement sensitivity of 6.76 nm/g. This results in a nominal capacitance of 9.0169 pF/g and differential capacitance change of 6.095 fF/g. The detailed dimensions of the accelerometer is shown in Table 1.

2.2 Accelerometer Employing Compliant Mechanism

Displacement amplifying mechanism provides an opportunity to improve the sensitivity of an accelerometer without increasing the device footprint. The layout of conventional and DaCM-based accelerometer is compared in Fig. 3. The DaCM-based accelerometer comprised of proof-mass assembly, DaCM, and sense combs. The proof-mass assembly drives the DaCM resulting in an amplified displacement of the sense combs. DaCM is characterized by inherent geometrical
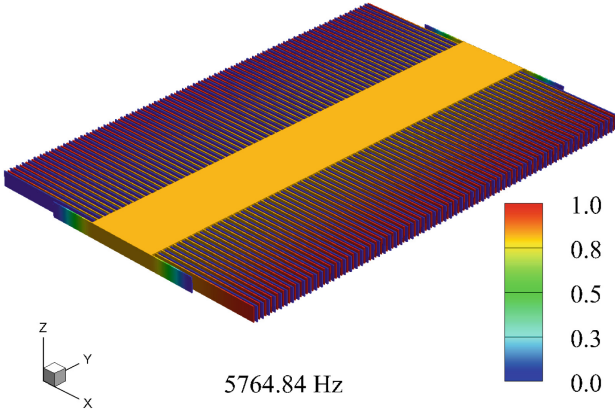
Fig. 2. A conventional accelerometer designed for a resonant frequency of 5.76 kHz with a footprint area of 2 mm × 3 mm

Table 1. Dimensions of conventional accelerometer

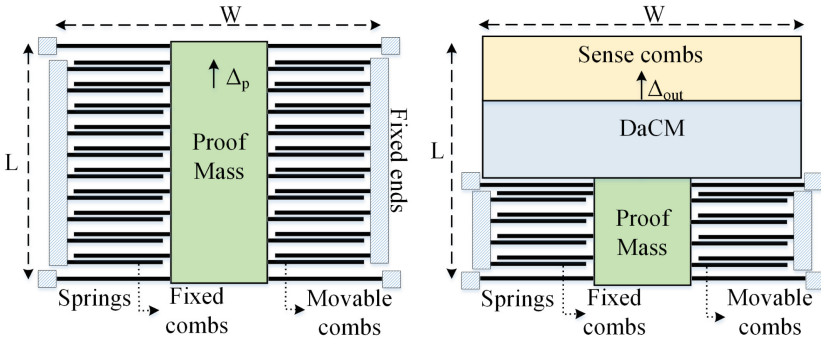|	Dimensions
Proof mass	3000 µm × 480 µm
Spring	319 µm × 7 µm
Combs	760 µm × 7 µm
Sense gap	10 µm
Comb pairs	67 × 2
Thickness	100 µm

Fig. 3. Illustration of DaCM-based accelerometer and a conventional accelerometer having the same footprint [16]

amplification $n = \frac{\Delta_{out}}{\Delta_{in}}$ and net amplification $NA = \frac{\Delta_{out}}{\Delta_p}$, where, Δ_p is displacement of the conventional accelerometer, Δ_{in} and Δ_{out} are the input and output displacement of DaCM respectively.

In literature, different compliant mechanisms have been reported. They have been implemented for technologies requiring ultra-high precision motion generation, such as scanning probe microscopes, mechanisms for nano-imprint lithography, precision manufacturing, cell manipulation, micro- grippers and optical steering mechanisms [12]. For applications like accelerometer, a higher net displacement amplification is desired. In [11], Krishnan et al. have presented a comparative study of the displacement amplification of different DaCM's for accelerometer application. The study shows that DaCM shown in Fig. 4 has relatively simple construction and a higher amplification [16]; and thus it is considered for analysis in this article. The two arms of the DaCM are fixed and force F_{in} is applied at the input node results in an input displacement of Δ_{in} and output displacement of Δ_{out}.
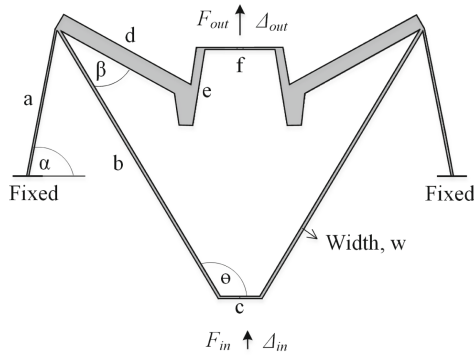

Fig. 4. Schematic of displacement amplifying compliant mechanism (DaCM). Here, a, b, c, d, e, f, w, α, β, and θ are the dimensional parameters.

Analysis of DaCM: The kinematics and the elastic deformation of the single-input-single-output compliant mechanisms can be expressed by the spring-leverage (SL) model, shown in Fig. 5, to account for its displacement-amplification [11]. In this model, five parameters are defined to fully characterize a compliant mechanism, i.e., input stiffness k_{ci}, output stiffness k_{co}, input mass m_{ci}, output mass m_{co}, and inherent geometrical amplification n. Analytical solutions to these parameters are challenging. Usually, finite element analysis (FEA) is used to estimate these parameters. In the first FEA run, a known force F_{in} is applied, keeping $F_{out} = 0$, to compute Δ_{in1}, and Δ_{out1}. The input stiffness k_{ci} and inherent geometrical amplification n is given as [11]

$$k_{ci} = \frac{F_{in}}{\Delta_{in1}} \tag{1}$$

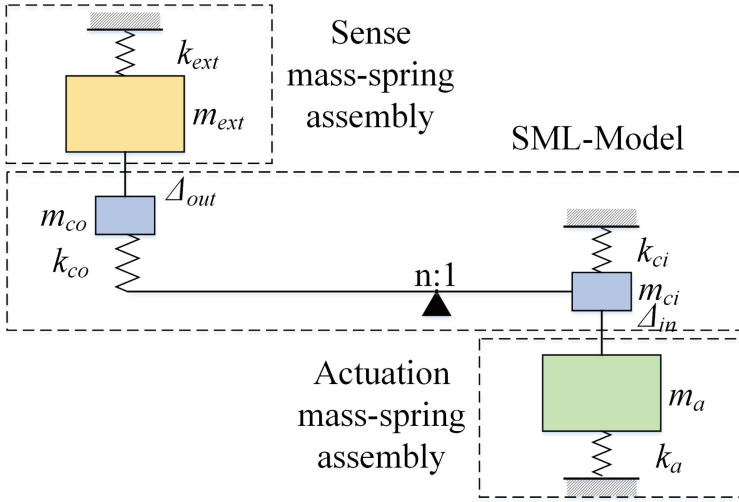$$n = \frac{\Delta_{out1}}{\Delta_{in1}} \tag{2}$$

Fig. 5. Spring-leverage model of compliant mechanism connected to actuator and sense-mass-spring assembly. Here, k_a and m_a are stiffness and mass of actuator, whereas k_{ext} and m_{ext} are stiffness and mass of the sense side. The DaCM parameters corresponding to stiffness (k_{ci}, k_{co}), inertial masses (m_{ci}, m_{co}), and inherent geometrical amplification n are also illustrated

In the next FEA run, a known force F_{out} is applied, keeping $F_{in} = 0$, to compute Δ_{in2} and Δ_{out2}. The output stiffness k_{co} can be given as [11]

$$k_{co} = \frac{F_{out}}{\Delta_{out2} - n\Delta_{in2}} \tag{3}$$

The estimation of input and out inertial masses of DaCM requires another FEA run where the first and the second modal frequencies are computed. Referring to Fig. 5, equations for modal frequencies are derived by first writing the Lagrangian for the system and then applying the Euler-Lagrange (E-L) equations to get [17]

$$\omega^2 = \left(\frac{k_{ci} + k_a + n^2 k_{co}}{2(m_{ci} + m_a)} + \frac{k_{ext} + k_{co}}{2(m_{co} + m_{ext})} \right)$$
$$\pm \sqrt{\left(\frac{k_{ci} + k_a + n^2 k_{co}}{2(m_{ci} + m_a)} - \frac{k_{ext} + k_{co}}{2(m_{co} + m_{ext})} \right)^2 + \frac{(nk_{co})^2}{(m_{co} + m_{ext})(m_{ci} + m_a)}} \tag{4}$$

The input-output inertial masses of DaCM are estimated by solving Eq. (4) for $k_a = m_a = k_{ext} = m_{ext} = 0$. The above discussed method is followed to estimate different parameters, i.e., n, k_{ci}, k_{co}, m_{ci}, and m_{co}, for the considered DaCM (shown in Fig. 4) and is presented in Table 2.

Table 2. Estimated parameters of the DaCM in Fig. 4

Parameters	FEA run 1	FEA run 2
Δ_{in}	1.2757 nm	1.1937 nm
Δ_{out}	9.9732 nm	11.994 nm
F_{in}	$9.81 \times 4.188 \times 10^{-7}$ N	$9.81 \times 5.025 \times 10^{-8}$ N
f_1	8.437 kHz	
f_2	10.567 kHz	
n	7.81	
k_{ci}	3217.24 N/m	
k_{co}	184.35 N/m	
m_{ci}	7.65×10^{-5} kg	
m_{co}	9.75×10^{-7} kg	

3   Optimization of DaCM

The design of displacement amplifying mechanism needs to be optimized for performance and footprint area. Further, feasibility of its fabrication using the existing technology also needs to be ensured. The optimization function for maximization of Δ_{out} can be defined as as a function of the geometrical parameters as

$$max(\Delta_{out}) = fun(a, b, c, d, e, f, \alpha, \beta, \theta, w) \qquad (5)$$
$$Constraints : w \geq w_{min} \qquad (6)$$

Equation (5) is constrained by permissible beam width w_{min}. The parametric optimization function available with FEA software, i.e., Coventor, COMSOL, IntelliSuite, can be used to study the variations of these parameters on Δ_{out}.

Typically, DaCM is classified as inverting and non-inverting type. In non-inverting type DaCM, Δ_{in} and Δ_{out} have displacements in the same direction, whereas it is in opposite directions for inverting DaCM. The DaCM in Fig. 4 is of non-inverting type. As shown in Fig. 7, increasing the length of beam b results in significant increase in Δ_{in} and Δ_{out}. However, for shorter beam length, displacement of Δ_{out} is reversed and DaCM becomes inverting. Thus, there is a trade-off between the DaCM displacements, and footprint area for its realization. The optimum dimensions of the different design parameters of DaCM estimated using FEA analysis are $a = 546\,\mu m$, $b = 1148\,\mu m$, $c = 160\,\mu m$, $d = 500\,\mu m$, $e = 115\,\mu m$, $w = 7\,\mu m$, $\alpha = 78.9°$, $\beta = 30°$, and $\theta = 121°$.

The optimized dimensions, presented above, are considered as reference for exploring the variations in design of DaCM as discussed below:

Curved beam: A curved microbeam with load across one end and fixed at other acts as a geometric anti-spring (GAS) structure, i.e., spring with significantly reduced stiffness. GAS has been incorporated in MEMS design to achieve higher

sensitivity for MEMS accelerometer and gravimeter [6,15]. In this section, analysis is presented to optimize the considered DaCM by exploiting curved beam based anti-spring geometry for beam a and b (see Fig. 6(a)). A Bezier polygon with quadratic function available in COMSOl Multiphysics is used for designing the curved beam. The curvature of beam a and b are varied by varying the parameter a_h and b_h, respectively, as shown in Table 3.

Table 3. Curvature of beam a and b with variations of a_h and b_h

a_h, b_h (µm)	0	10	20	30	40	50	60	70	80	90	100	110	120	130	140	150	160	170	180	190
Curvature of beam a $\left(\tan^{-1}\left(\frac{a_h}{0.5a}\right)\right)$, in deg)	0	2.1	4.2	6.3	8.3	10.4	12.4	14.4	16.3	18.2	20.1	21.9	23.7	25.5	27.2	28.8	30.4	31.9	33.4	34.8
Curvature of beam b $\left(\tan^{-1}\left(\frac{b_h}{0.5b}\right)\right)$, in deg)	0	1	2	2.99	3.99	4.98	5.97	6.95	7.93	8.91	9.88	10.85	11.81	12.76	13.71	14.65	15.58	16.5	17.41	18.32

The variations of input and output displacements, i.e., Δ_{in}, Δ_{out}, of DaCM with curved beams for an applied input boundary load is shown in Fig. 6. As shown in Fig. 6(b), Δ_{in} increases with increasing curvature of beam b, however, it decreases with the curvature of beam a. This is because the anti-spring design of beam b reduces its stiffness and allows larger displacement of Δ_{in}. Thus, the combination of straight beam a and curved beam b have maximum Δ_{in} displacement. Further, it is also observed that Δ_{out} increases significantly with the curvature of beam b and remains nearly independent to the curvature of beam a (see Fig. 6c)). Thus, it can be argued replacing straight beam b with a curved beam in the design of DaCM, shown in Fig. 4, increases the input and output displacements. In addition to the input and output displacements, an important parameter defined to characterize a DaCM is inherent geometrical amplification n. It is defined as the ratio of Δ_{out} by Δ_{in}. Interestingly, a higher value of n is observed for straight beams based design of DaCM, i.e., $a_h = b_h = 0$ (see Fig. 6(d))). However, Δ_{in} and Δ_{out} are relatively less for straight beam based design compared to the curved beam DaCM design. This is further evident from the total displacement plot shown in Fig. 6(e)). The curved beam based design has higher total displacement, which is the sum of Δ_{in} and Δ_{out}. Thus, it can be concluded that a higher inherent geometrical amplification should not be the main criteria in the choice of DaCM as it does not guarantee a larger input-output displacements.

Variations of curved beam design: Different variations of the curved beam based DaCM have also been explored, i.e., *inverted curved beam*, and *double curved beam design*. The inverted curved beam DaCM, shown in Fig. 8(a) has curvature of beam b in opposite direction to the curved beam DaCM. The double curved beam design of DaCM is shown in Fig. 8(c). This design is the combination of the curved and inverted curved DaCM design. For brevity, a detailed analysis of inverted curved and double curved beam DaCM designs is not presented. However, in the next section, a comparative analysis of the designed accelerometer using these designs are included.

In the next section, the design of accelerometer using compliant mechanism is presented.
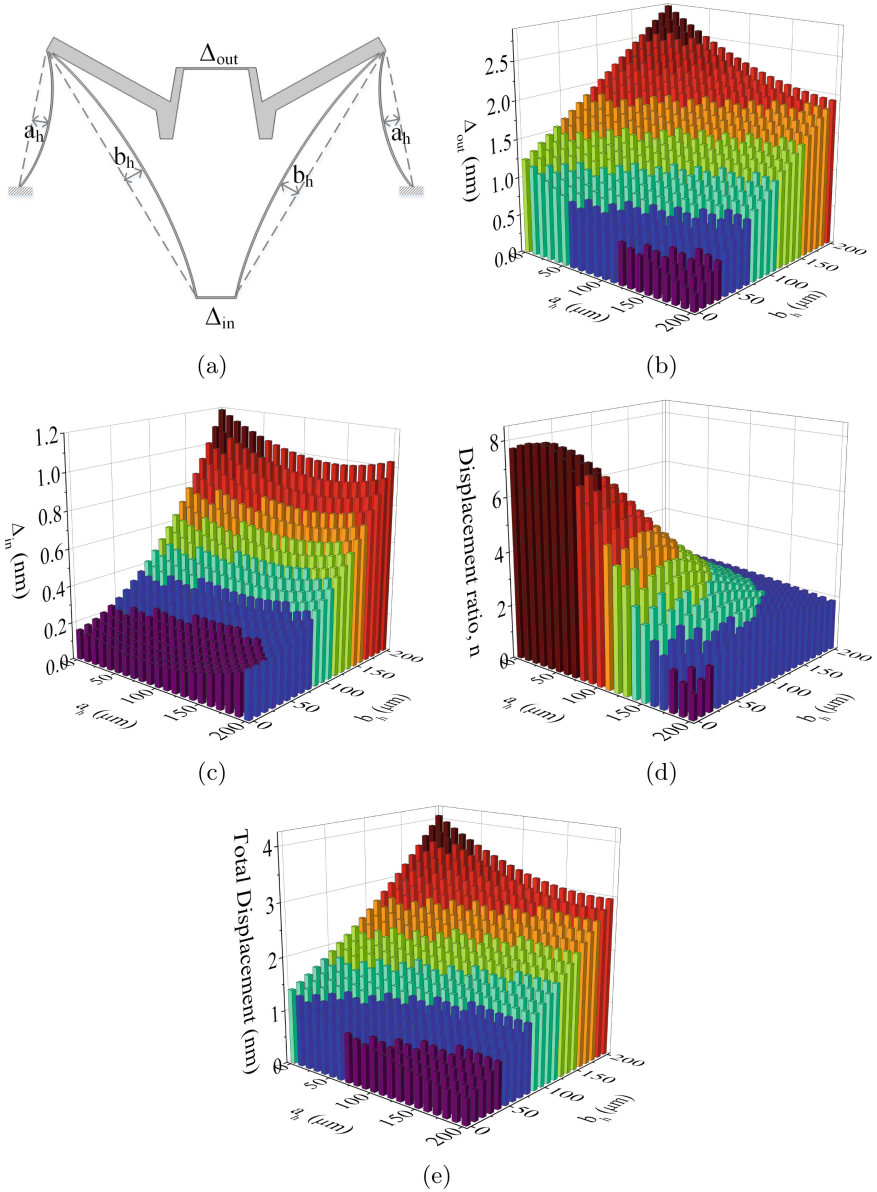
(a)

(b)

(c)

(d)

(e)

Fig. 6. Analysis of curved beam based DaCM design: (a) Schematic of curved beam DaCM; displacement of Δ_{out} and Δ_{in} are shown in (b) and (c), respectively, for different curvature of beam a and b. Displacement ratio, i.e., $n = \frac{\Delta_{out}}{\Delta_{in}}$ and total displacement, i.e., $(\Delta_{in} + \Delta_{out})$, are presented in (d) and (e) respectively
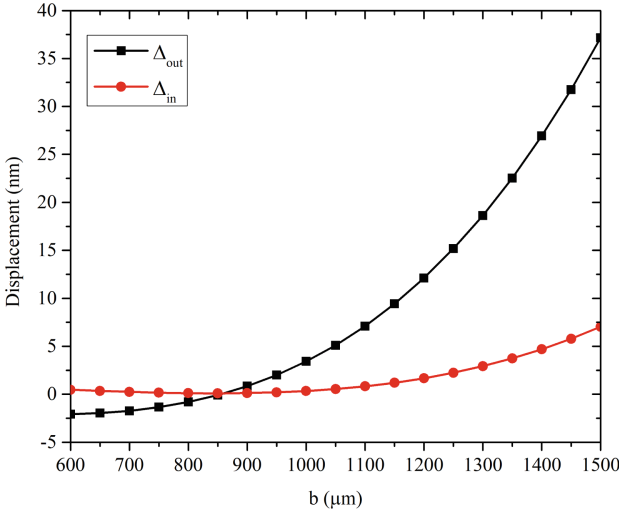
Fig. 7. Displacements of Δ_{out} and Δ_{in} with parametric variation of beam length b

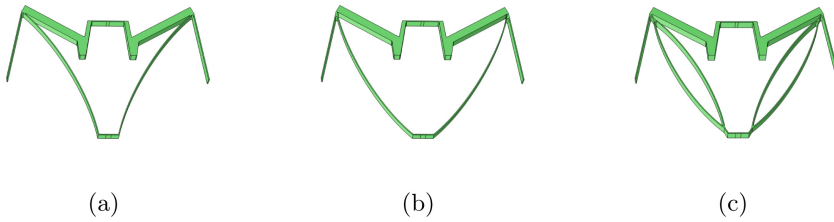|		
(a)	(b)	(c)

Fig. 8. Schematic of different DaCM designs: (a) Curved beam, (b) Inverted curved beam and (c) Double curved beam design

4 Accelerometer Using Compliant Mechanism

The schematic of accelerometers with straight and curved beam based DaCM is shown in Fig. 9. The accelerometer consists of a proof-mass of $1500\,\mu m \times 1000\,\mu m$ suspended by springs of $700\,\mu m \times 7\,\mu m$ for driving the compliant structure. The amplified displacement Δ_{out} drives the sense comb assembly resulting in larger sense gap variations and sensitivity improvement. The sense gap of the combs is $10\,\mu m$. The sense mass has a dimension of $1000\,\mu m \times 50\,\mu m$ and is supported by springs of $500\,\mu m \times 7\,\mu m$. The proof mass and the sense mass have 68 and 38 pairs of electrodes, respectively, of size $600\,\mu m \times 7\,\mu m$. The thickness of the structure considered for the analysis is $100\,\mu m$ and the device footprint area is $2\,mm \times 3\,mm$. The analysis considers polycrystalline silicon as structural material with Young's modulus of $160\,GPa$, density of $2330\,kg/m^3$.
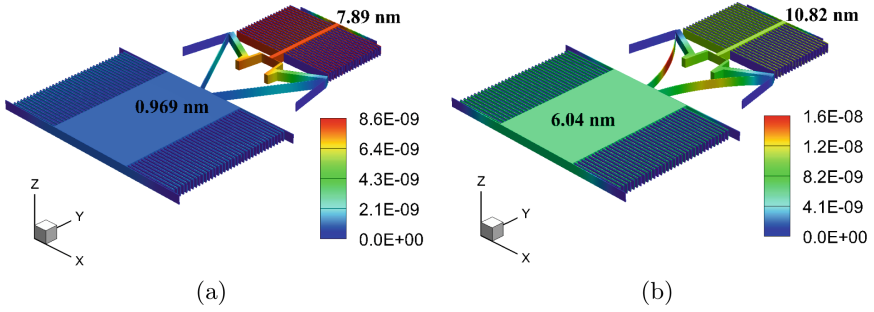
Fig. 9. Displacement sensitivity of (a) Straight beam DaCM, and (b) Curved beam DaCM based accelerometer design for applied acceleration of $1g$ along Y-axis. Accelerometer in (a) and (b) have resonant frequencies of $7.09\,\mathrm{kHz}$ and $5.875\,\mathrm{kHz}$, respectively, for the same dimensions
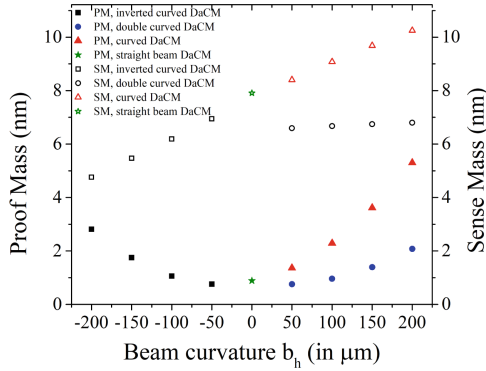

Fig. 10. Displacement sensitivity of accelerometer with different DaCM, i.e., straight beam, curved beam, inverted curved beam, and double curved beam, are compared for and applied load of $1g$

Figure 10 shows the comparison of the proof mass and the sense mass displacement for the different compliant mechanism based accelerometers. These displacements are estimated for an applied acceleration of $1g$. Analysis shows the straight beam DaCM has a sense mass displacement of $7.89\,\mathrm{nm}$. The amplified sense mass displacement decreases with the curvature of the inverted curved beam DaCM (Fig. 8(b)). However, for a curved beam design, the sense mass displacement increases with the curvature of beam b. In case of the double curved beam design, the sense mass displacement remains same with increasing the curvature of the beams. Thus, it can be concluded that the curved beam DaCM outperforms the other DaCM variants in terms of the amplified sense mass displacement. Hence, it is preferred and considered for further analysis in the next section.

5   Results and Discussion

In this section, different parameters, i.e., modal frequencies, displacements for applied acceleration, stress, non-linearity, and capacitance charges, of the designed straight and curved beam DaCM based accelerometer are compared.

5.1   Modal Frequencies

The modal analysis of the accelerometer is carried out in CoventorWare. The design with straight and curves beam DaCM have in-plane displacement with the first modal frequency at 7.09 kHz and 5.875 kHz respectively. As the same dimensions are considered for both designs, it is apparent that the curved beam based DaCM reduces the overall stiffness of the design and thus results in resonant frequency reduction. The displacement sensitivity and modal frequencies of the straight and curved beam DaCM based accelerometer is shown in Fig. 9.

5.2   Cross-Axis Sensitivity

Cross-axis sensitivity is a measure of output observed across one axis when the acceleration is imposed on a different axis. The proposed accelerometer is exposed to an acceleration of $1g$, $10g$, and $30g$ along Y-axis and the cross axis sensitivity along X-axis and Z-axis are determined. The estimated cross-axis sensitivity along X-axis and Y-axis are $\sim 0.003\%$ and $\sim 0.005\%$, respectively, for the sense mass displacement of both types of accelerometer. This suggests that the curved beam based compliant design of does not contribute to the cross-axis sensitivity.

5.3   Stress

The stress gradient in the accelerometer must be less than the yield strength of the silicon. Typically, the yield strength of silicon is around 165 MPa [18]. The stress gradients shown in Fig. 11 is calculated for an applied body load of $100g$. The straight beam and curved beam DaCM based accelerometer have a maximum stress concentration of 11 MPa and 15 MPa respectively, which is less compared to the yield stress of silicon. This ensures the reliable operation of the designed accelerometer.

5.4   Non-linearity

The design of an accelerometer must ensure that the non-linearity in the displacement of the movable masses are minimum over the range of their operation. A compliant mechanism based accelerometer must ensure that the both the proof mass displacement and the amplified sense mass displacement are liner the over desired range. The non-linearity is studied by estimating the deviations in the displacement of the masses with reference to the extrapolated linear displacement for varying acceleration. As shown in Fig. 12, the simulated and the
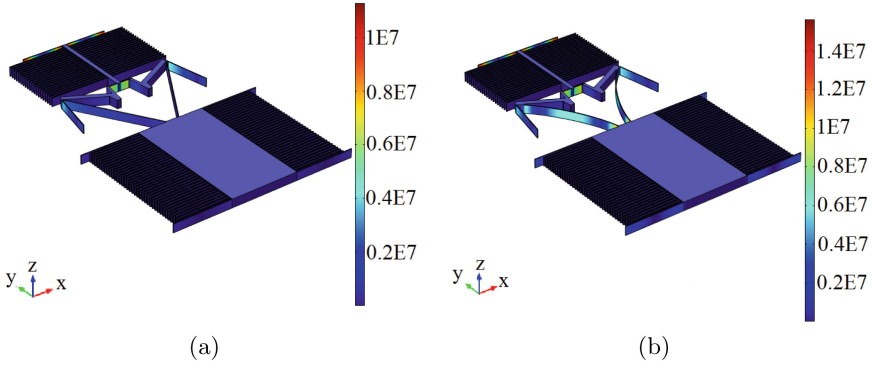
Fig. 11. Stress analysis for an applied body load of 100g: (a) Straight beam, and (b) Curved beam DaCM based accelerometer
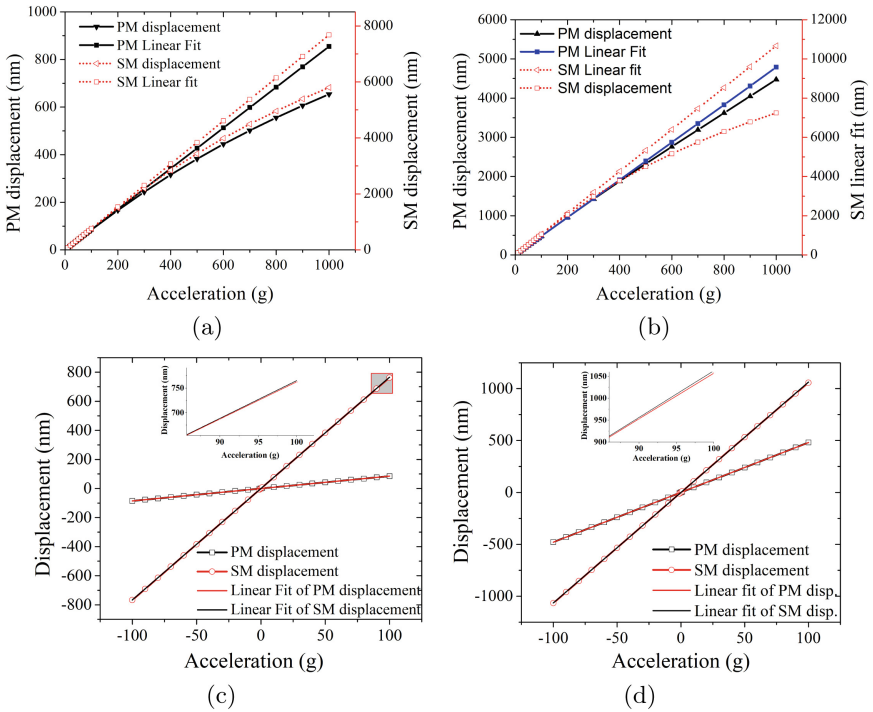

Fig. 12. Non-linearity in displacement of proof mass (PM, before amplification) and sense mass (SM, after amplification) over applied acceleration: (a), (c) Straight beam, and (b), (d) Curved beam based DaCM. The non-linearity is 1.345% and 2.739% for straight and curved beam based accelerometer over a range of 100g

linearly fitted displacement of the sense masses has a non-linearity of 1.345% and 2.739% for straight and curved beam based accelerometer over a range of $100g$. An increase in applied acceleration increases the displacement deviation from the linear fit line and thus the non-linearity increases. This observed trend is same for both straight beam and curved beam DaCM based accelerometer.

5.5   Capacitance

The proof mass has a smaller displacement, however it can accommodate a larger comb pairs across its length. The proof mass has 68 comb pairs and can be used for actuation purpose. The capacitive sensitivity of the proof mass comb pairs are $1.2\,\mathrm{fF/g}$ and $4.1\,\mathrm{fF/g}$ respectively for the accelerometer with straight beam and curved beam DaCM. Incorporating DaCM in the design amplifies the output displacement of the sense mass. This allows larger capacitive sensitivity for sense mass comb pairs. The considered design has a sense mass electrodes count of 38. This gives the output capacitive sensitivity of $3.4\,\mathrm{fF/g}$ and $4.4\,\mathrm{fF/g}$ respectively for the sense mass comb pairs of the accelerometer with straight beam and curved beam DaCM.

Table 4. Simulated parameters of accelerometers in Fig. 9

Parameters	Design in Fig. 9(a)	Design in Fig. 9(b)
Resonant frequency, kHz	7.09	5.875
Input displacement sensitivity, nm/g	0.969	6.04
Output displacement sensitivity, nm/g	7.89	10.82
Geometrical amplification	8.14	1.79
Cross-axis sensitivity	$S_{YX}=0.003\%,\ S_{YZ}=0.005\%$	
Stress at $100g$, MPa	11	15
Non-linearity (%, for $\pm100g$)	1.345	2.739
Proof mass electrode nominal capacitance, pF	7.4383	
Sense mass electrode nominal capacitance, pF	4.7694	

6   Analysis of Fabrication Induced Variations

Silicon-on-insulator (SOI) based micro-fabrication is a four mask process, i.e., PAD METAL, SOI, TRENCH, and BLANKET METAL. The PAD METAL mask is used to deposit a layer of 20 nm chrome and 500 nm gold on the silicon and is used for interconnects. The patterning of silicon is carried out using SOI mask layer. Accordingly, the silicon layer is etched out using DRIE (Dry reactive ion etch) to realize the required geometry. Next, it is ensured that the designed structure is properly released. This is ensured by removing the substrate and oxide layer beneath the structure using the TRENCH mask. In the end, bond

pads are realized using the BLANKET METAL mask. These bond pads are used for electrical connections during the packaging of the fabricated devices.

Ideally, the etched silicon layer should have a steep vertical (orthogonal) faces. Practically, the etched silicon faces are slanted. The slanting depends on the thickness of the silicon layer. Typically, a $100\,\mu$m thick silicon layer has a sidewall slanting angle of an order of 0.8° [19]. This results in non-uniform width variations across the thickness of the silicon layer. As a result, the stiffness of the springs used to suspend the proof mass is changed. The variation in stiffness of the spring, induced due to the fabrication process, has a significant effect the resonant frequencies and other performance parameters of the devices.
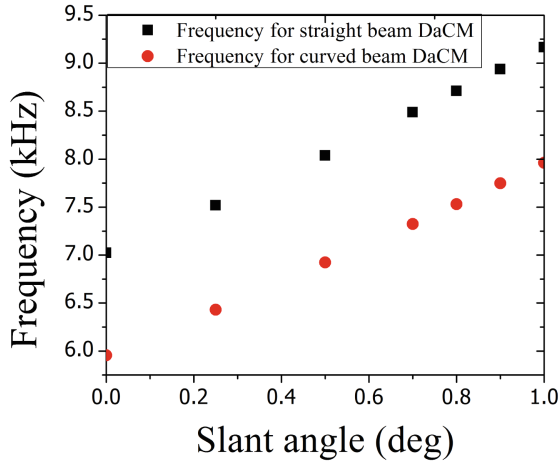

Fig. 13. Effect of sidewall angle due to fabrication process on resonant frequency

7   Conclusion

Curved beam based displacement amplifying compliant mechanism, inspired from the geometrical anti-spring design, has been explored in this article. A detailed analysis of the curved beam DaCM is presented and compared to the conventional straight beam DaCM. Despite having a lesser geometrical amplification ratio, the curved beam DaCM has a larger sense mass displacement. This is because of the lower input stiffness of the curved beam DaCM which allows a lager proof mass displacement. Other variations of the curved beam DaCM, i.e., inverted curved beam, and double curve beam DaCM, are also studied and compared. The curved beam DaCM design outperforms the other DaCM designs and has a larger proof mass and the sense mass displacements. Further, a detailed analysis of the complete accelerometer design using the curved beam DaCM is also presented and different performance parameters like modal frequencies,

cross-axis sensitivity, stress, and non-linearity are estimated. The effect of the fabrication tolerances by considering the side-wall angle during dry reactive ion etching is also studied. Analysis suggests that an increase in side-wall angle increases the resonant frequency of the designed accelerometer. In future, we plan to fabricate the designed accelerometer and characterize.

References

1. Tanaka, M.: An industrial and applied review of new mems devices features. Microelectron. Eng. **84**(5–8), 1341–1344 (2007)
2. Barbour, N.M.: Inertial Navigation Sensors. Tech. Rep, Charles Stark Draper Laboratory, Cambridge MA, USA (2010)
3. Handtmann, M., Aigner, R., Meckes, A., Wachutka, G.K.: Sensitivity enhancement of mems inertial sensors using negative springs and active control. Sens. Actuators A Phys. **97**, 153–160 (2002)
4. Gabrielson, T.B.: Mechanical-thermal noise in micromachined acoustic and vibration sensors. IEEE Trans. Electron Dev. **40**(5), 903–909 (1993)
5. Khan, S., Ananthasuresh, G.: Improving the sensitivity and bandwidth of in-plane capacitive microaccelerometers using compliant mechanical amplifiers. J. Microelectromech. Syst. **23**(4), 871–887 (2014)
6. Zhang, H., Wei, X., Ding, Y., Jiang, Z., Ren, J.: A low noise capacitive mems accelerometer with anti-spring structure. Sens. Actuators A Phys. **296**, 79–86 (2019)
7. Zhang, H., Li, B., Yuan, W., Kraft, M., Chang, H.: An acceleration sensing method based on the mode localization of weakly coupled resonators. J. Microelectromech. Syst. **25**(2), 286–296 (2016)
8. L.L. Howell, Compliant mechanisms. In: 21st Century Kinematics, pp. 189–216. Springer (2013)
9. Zeimpekis, I., Sari, I., Kraft, M.: Characterization of a mechanical motion amplifier applied to a MEMS accelerometer. J. Microelectromech. Syst. **21**, 1032–1042 (2012)
10. Hetrick, J., Kota, S.: An energy formulation for parametric size and shape optimization of compliant mechanisms (1999)
11. Krishnan, G., Ananthasuresh, G.: Evaluation and design of displacement-amplifying compliant mechanisms for sensor applications. J. Mech. Des. Trans. ASME **130**(10), 1023041–1023049 (2008)
12. Iqbal, S., Malik, A.: A review on mems based micro displacement amplification mechanisms. Sens. Actuators A Phys. **300**, 111666 (2019)
13. Boom, B.A., Bertolini, A., Hennes, E., Brookhuis, R.A., Wiegerink, R.J., Brand, J.F.V.D., Beker, M.G., Oner, A., Wees, D.V.: Nano-g accelerometer using geometric anti-springs. In: Proceedings of the IEEE International Conference on Micro Electro Mechanical Systems (MEMS), vol. 2, pp. 33–36 (2017)
14. Mansouri, B.E., Middelburg, L.M., Poelma, R.H., Zhang, G.Q., van Zeijl, H.W., Wei, J., Jiang, H., Vogel, J.G., van Driel, W.D.: High-resolution MEMS inertial sensor combining large-displacement buckling behaviour with integrated capacitive

readout. Microsyst. Nanoeng. **5** (2019.) [Online]. Available: https://doi.org/10.1038/s41378-019-0105-y

15. Middlemiss, R., Samarelli, A., Paul, D., Hough, J., Rowan, S., Hammond, G.: Measurement of the earth tides with a mems gravimeter. Nature **531**(7596), 614–617 (2016)

16. Khan, S.: Development of micromachined and meso-scale multi-axis accelerometers with displacement-amplifying compliant mechanisms. Ph.D. dissertation, Citeseer (2013)

17. Hegde, S., Ananthasuresh, G.: A spring-mass-lever model, stiffness and inertia maps for single-input, single-output compliant mechanisms. Mech. Mach. Theory **58**, 101–119 (2012)

18. Silicon - strength - hardness - elasticity - crystal structure, Nov 2020. [Online]. Available: www.material-properties.org/silicon-mechanical-properties-strength-hardness-crystal-structure/

19. Biswas, A., Pawar, V.S., Menon, P.K., Pal, P., Pandey, A.K.: Influence of fabrication tolerances on performance characteristics of a mems gyroscope. Microsyst. Technol. **27**(7), 2679–2693 (2021)